The Astrophysical Journal, 598:993–999, 2003 December 1
© 2003. The American Astronomical Society. All rights reserved. Printed in U.S.A.

THEORY OF PIXEL LENSING TOWARD M31. II. THE VELOCITY ANISOTROPY AND FLATTENING OF THE MACHO DISTRIBUTION

E. Kerins,[1] J. An,[2] N. W. Evans,[2] P. Baillon,[3] B. J. Carr,[4] Y. Giraud-Héraud,[5] A. Gould,[6] P. Hewett,[2] J. Kaplan,[5] S. Paulin-Henriksson,[5] S. J. Smartt,[2] Y. Tsapras,[4] and D. Valls-Gabaud[7]
(The POINT-AGAPE Collaboration)
Received 2003 April 1; accepted 2003 August 8

ABSTRACT

The POINT-AGAPE collaboration is currently searching for massive compact halo objects (MACHOs) toward the Andromeda galaxy (M31). The survey aims to exploit the high inclination of the M31 disk, which causes an asymmetry in the spatial distribution of M31 MACHOs. Here, we investigate the effects of halo velocity anisotropy and flattening on the asymmetry signal using simple halo models. For a spherically symmetric and isotropic halo, we find that the underlying pixel lensing rate in far-disk M31 MACHOs is more than 5 times the rate of near-disk events. We find that the asymmetry is further increased by about 30% if the MACHOs occupy radial orbits rather than tangential orbits, but it is substantially reduced if the MACHOs lie in a flattened halo. However, even for halos with a minor- to major-axis ratio of $q = 0.3$, the number of M31 MACHOs in the far side outnumber those in the near side by a factor of $\sim$2. There is also a distance asymmetry, in that the events on the far side are typically farther from the major axis. We show that, if this positional information is exploited in addition to number counts, then the number of candidate events required to confirm asymmetry for a range of flattened and anisotropic halo models is achievable, even with significant contamination by variable stars and foreground microlensing events. For pixel lensing surveys that probe a representative portion of the M31 disk, a sample of around 50 candidates is likely to be sufficient to detect asymmetry within spherical halos, even if half the sample is contaminated, or to detect asymmetry in halos as flat as $q = 0.3$, provided less than a third of the sample comprises contaminants. We also argue that, provided its mass-to-light ratio is less than 100, the recently observed stellar stream around M31 is not problematic for the detection of asymmetry.

Subject headings: dark matter — galaxies: individual (M31) — gravitational lensing

1. INTRODUCTION

Continuing disagreement as to whether massive compact halo objects (MACHOs) have been detected by microlensing experiments looking toward the Magellanic Clouds highlights the need for other microlensing targets (e.g., Kerins 2001). The Andromeda galaxy (M31) presents an opportune target in this respect. The disk of M31 is highly inclined ($i \sim 77°$), with the consequence that lines of sight to disk stars in the northwest or near side of M31 are shorter than those to the southeast or far side. Microlensing by a spheroidal dark halo will have a characteristic signature with an excess of events on the far side of the M31 disk (Crotts 1992; Baillon et al. 1993). This asymmetric signal is absent for variable stars or stellar microlenses in the disk of M31. A number of groups (e.g., Aurière et al. 2001; Riffeser et al. 2001; Calchi-Novati et al. 2002; Crotts et al. 2001) are now carrying out large-scale surveys of M31 to search for this near-far disk asymmetry. This is a mammoth task as the individual stars in M31 are not resolved, so that new techniques based on the superpixel method (Ansari et al. 1997) or difference imaging (e.g., Crotts & Tomaney 1996) have been exploited to measure the flux changes on unresolved stars. Nonetheless, convincing candidate events are now being discovered, for example, by the POINT-AGAPE collaboration (e.g., Aurière et al. 2001; Paulin-Henriksson et al. 2002, 2003). Therefore, this is a timely moment to consider what factors affect the near-far disk asymmetry and how many events are likely to be needed for a convincing detection.

The aim of this paper is to estimate the size of candidate event samples needed to detect asymmetry for different halo models. In §§ 2 and 3 of the paper we show how the magnitude of the asymmetry signal is affected by the velocity anisotropy and the flattening of the M31 baryonic dark halo, respectively. There are few ways known to us for measuring the properties of the orbits of dark objects in the halo of any galaxy or for ascertaining the flattening of the baryonic dark component of the halo. Hence, any clues gleaned from pixel lensing experiments will be invaluable. In § 4, we present some simple, nonparametric statistical estimators of asymmetry and calculate how many candidates are needed to give convincing detections.

2. THE EFFECTS OF VELOCITY ANISOTROPY

2.1. *Anisotropic Models*

Here, we investigate the microlensing properties of halos in which the velocity distribution of the MACHOs is

[1] Astrophysics Research Institute, Liverpool John Moores University, Egerton Wharf, Birkenhead CH41 1LD, UK.
[2] Institute of Astronomy, University of Cambridge, Madingley Road, Cambridge CB3 0HA, UK.
[3] European Organization for Nuclear Research (CERN), 1211 Geneva 23, Switzerland.
[4] Astronomy Unit, School of Mathematical Sciences, Queen Mary, University of London, Mile End Road, London E1 4NS, UK.
[5] Laboratoire de Physique Corpusculaire et Cosmologie, Collège de France, 11 Place Marcelin Berthelot, F-75231 Paris, France.
[6] Department of Astronomy, Ohio State University, 140 West 18th Avenue, Columbus, OH 43210.
[7] Laboratoire d'Astrophysique UMR CNRS 5572, Observatoire Midi-Pyrénées, 14 Avenue Edouard Belin, F-31400 Toulouse, France.

anisotropic. We use models in which the halo density ρ is isothermal and the rotation curve is flat,

$$\rho \propto \frac{v_0^2}{r^2} , \quad v_0^2 = \text{constant} . \tag{1}$$

For these models, the velocity dispersions in the spherical polar coordinate system are given by (see, e.g., White 1981; Evans, Häfner, & de Zeeuw 1997)

$$\sigma_\phi^2 = \sigma_\theta^2 = (1+\alpha)\sigma_r^2 = \frac{v_0^2}{2} , \tag{2}$$

where $\alpha > -1$ is the anisotropy parameter. If $\alpha < 0$, then the velocity distribution is referred to as "radially anisotropic"; if $\alpha > 0$, then it is "tangentially anisotropic." While σ_r^2 in equation (2) diverges as $\alpha \to -1$, velocity dispersion ratios are rarely observed to be more extreme than 3 : 1, implying $-8/9 < \alpha < 8$. We assume a circular velocity of $v_0 = 235$ km s^{-1} for the M31 halo (Emerson 1976), and we compute the cutoff radius to give a total halo mass of $1 \times 10^{12}\ M_\odot$ (e.g., Evans & Wilkinson 2000). The sources are drawn from the M31 disk, which is adequately modeled as a sheet inclined at 77° to the line of sight. The source velocity is assumed to be dominated by the disk rotation speed of 235 km s^{-1}.

For each halo model, we calculate a theoretical estimate of the pixel lensing rate Γ_p. Unlike the classical (resolved star) microlensing rate, Γ_p depends additionally on the surface brightness of the M31 disk and the luminosity function of the M31 sources (see Kerins et al. 2001). The calculations here are performed for a V-band luminosity function and surface brightness distribution. The surface brightness of M31 is tabulated in Walterbos & Kennicutt (1987). The M31 disk luminosity function is assumed to be the same as for the Milky Way, and we use the data of Wielen, Jahreiss, & Krüger (1983) to characterize the faint end ($M_V > 5$) and that of Bahcall & Soneira (1980) for the bright end. For each source star of flux F at sky position (x, y) on the M31 disk, we compute the maximum impact parameter, u_T, needed to ensure that the magnified source star noticeably enhances the local flux contribution from the background galaxy and sky background. Motivated by the POINT-AGAPE experiment (e.g., Paulin-Henriksson et al. 2002, 2003), we assume that detection is performed on a "superpixel" array of pixels of size $2\farcs1 \times 2\farcs1$, which typically encloses 40% of the total flux from a point source. In addition to the background due to the M31 surface brightness, we allow for a sky background of 19.5 mag arcsec^{-2}. We assume an event is detectable if the flux change caused by microlensing is $\gtrsim 1\%$ of the background flux on the superpixel. The pixel lensing rate is then

$$\Gamma_p(x,y) = \langle u_T(x,y)\rangle \Gamma_c(x,y) , \tag{3}$$

where Γ_c is the classical microlensing rate (Paczyński 1986; Kiraga & Paczyński 1994) and $\langle u_T\rangle$ is the maximum impact parameter averaged over the luminosity function ϕ of the source stars. Explicitly, we can write that

$$\langle u_T(x,y)\rangle = \frac{\int \phi(F) u_T(F,x,y)\, dF}{\int \phi(F)\, dF} . \tag{4}$$

This is an upper limit to the observed pixel lensing rate for any real experiment, as it does not take into account the effects of sampling, changing observing conditions, or event identification algorithms. These effects may alter the spatial distribution of events, but they can be corrected via the calculated detection efficiency. In fact, the efficiency is largely controlled by the local surface brightness and so is approximately symmetric with respect to the major axis. The ratio of the number of far-disk to near-disk events therefore does not depend on the efficiency to lowest order.

Finally, the spatially averaged pixel lensing rate $\langle \Gamma_p \rangle$ is obtained by weighting the rate with the M31 disk surface brightness. The central portions of the M31 disk are omitted, partly because stellar lenses in the M31 bulge dominate here and partly because the halo model is singular at the center. Thus, a central region of 5′ radius is excised from the M31 disk before performing the spatial averaging separately for events above and below the M31 major axis. None of the current experiments is surveying the entire M31 disk, but their fields do span the large majority of the minor axis, and we therefore expect any underlying asymmetry in their fields to be representative of the globally averaged asymmetry computed here.

2.2. *Results*

Figure 1 shows the spatially averaged theoretical pixel lensing rate, $\langle \Gamma_p \rangle$, for lenses of mass M, normalized to the value $\Gamma_0 = 7.6 \times 10^{-7} (M/M_\odot)^{-1/2}$ events per star per year. When $\alpha < 0$, the velocity distribution is radially anisotropic and the rate $\langle \Gamma_p \rangle \propto v_0/(1+\alpha)^{1/2}$. When $\alpha > 0$, the velocity distribution is tangentially anisotropic and the rate $\langle \Gamma_p \rangle \propto v_0$, so the total rate in radially anisotropic models is somewhat higher. However, we are primarily interested in the differences between the near and far disk. Such asymmetries may manifest themselves in the numbers, locations, and timescales of the events. Accordingly, Figure 1 also shows the far- to near-disk ratios for the pixel lensing rates ($A = \langle \Gamma_p \rangle_f / \langle \Gamma_p \rangle_n$), the mean Einstein crossing times ($\langle t_E \rangle_f / \langle t_E \rangle_n$), and the ratio of mean projected distances of events to the major axis (D).

All models show a strong excess of far-disk events, with A increasing from 5.3 to 7 as the models go from tangential to radial anisotropy. It is also evident from D in Figure 1 that

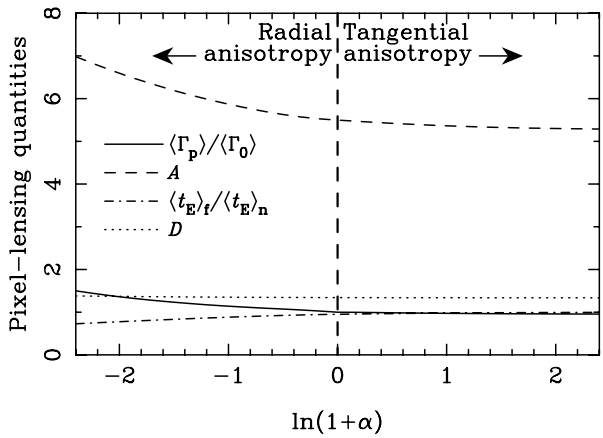


FIG. 1.—Spatially averaged pixel lensing rate $\langle \Gamma_p \rangle$ (*solid line*) as a function of anisotropy parameter α and normalized to the value for the isotropic model $\langle \Gamma_0 \rangle = 7.6 \times 10^{-7}$ star^{-1} yr^{-1}. Also shown is the M31 MACHO number asymmetry A (*dashed line*), the ratio of near-disk to far-disk average durations $\langle t_E \rangle_f / \langle t_E \rangle_n$ (*dot-dashed line*), and the ratio of projected distances to the major axis D (*dotted line*).

far-disk events lie systematically farther from the major axis than near-disk events, providing a second signature of asymmetry. However, D is nearly constant across the range of α, so this spatial signature does not provide a probe of the degree of velocity anisotropy.

There is also an asymmetry in the Einstein crossing times of M31 MACHOs. If MACHOs have radially distended orbits, then their motion tends toward being parallel to the line of sight for the near disk but being orthogonal to it for the far disk. Events on the near side therefore last longer. In other words, the ratio of the typical timescales of far-disk to near-disk events decreases with increasing radial anisotropy. Consequently, the ratio of the numbers of events in the far disk to the near disk is enhanced in radially anisotropic models compared to isotropic models. This can be seen from the fact that the spatially averaged microlensing optical depth, $\langle\tau\rangle \propto \langle t_{\rm E}\rangle\langle\Gamma_p\rangle$, is independent of the velocity distribution. From Figure 1, the expected enhancement in the number asymmetry A is $\sim$30%.

For the isotropic model ($\alpha = 0$), the timescales are typically shorter in the far disk than in the near disk. The reason for this is that the typical separation between lens and source is larger for near-disk MACHOs. For far-disk events, the typical lens-source separation is biased toward the location where the density peaks along the line of sight, which is at a distance $\sim|y|\tan i$ in front of the sources, where y is the projected distance along the minor axis. The situation is different for near-disk MACHOs, where the line-of-sight density is always a monotonically decreasing function of lens-source separation. Here, the typical separation is $\sim$20–30 kpc for $y > 5'$, so $\langle t_{\rm E}\rangle_f/\langle t_{\rm E}\rangle_n$ is less than unity for an isotropic model, as shown in Figure 1.

Unfortunately, the Einstein crossing time is not generally measurable for pixel lensing events. Instead, experiments measure the FWHM ($t_{1/2}$) of the light curve, which is additionally correlated with the source luminosity and background surface brightness distribution. The resulting $t_{1/2}$ distributions are therefore predicted to be broad, and any asymmetries in the timescale distribution are unlikely to be easily observable.

3. THE EFFECTS OF FLATTENING

3.1. *Flattened Models*

Self-consistent solutions of the self-gravitation equations for the density, potential, and velocity distributions of flattened halo models are rare. Even solving the Jeans equations for the second velocity moments can lead to cumbersome results. Baltz, Gyuk, & Crotts (2003) have computed pixel lensing rates explicitly for simple analytic flattened halo models. However, if we are merely interested in comparing the effects of flattening on the ratios of quantities in the near and far disk, then there is a quick alternative to carrying out computations with a fully axisymmetric halo model.

Figure 2 shows lines of sight passing through an elliptical halo with an axis ratio q and eccentricity $(1 - q^2)^{1/2}$. The lines strike the disk of M31 at an angle i. The ratios of the optical depths in the near and far disk are proportional to the line segments NP and FP. Also shown is an equivalent spherical halo. By extending N vertically to N$'$ and F to F$'$, we can construct lines of sight that pass through the spherical halo and strike the disk at a different angle i'. Similarly,

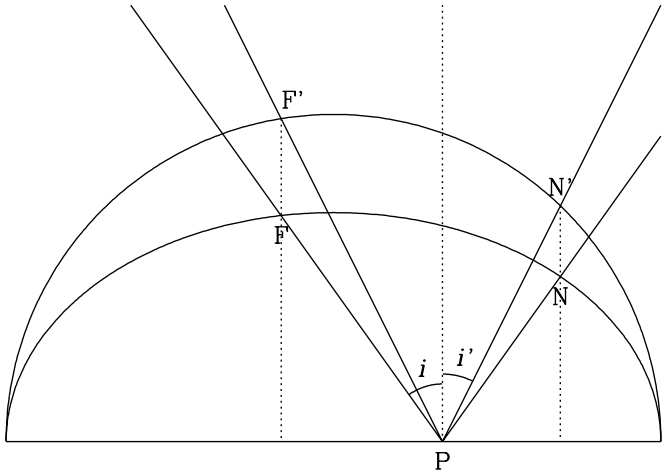


FIG. 2.—Shows lines of sight through a spherical and an elliptical halo. From the properties of an ellipse, we know that the ratios NP : FP and N$'$P : F$'$P are equal. This enables us to relate the asymmetry signal of a disk viewed through a flattened halo at inclination i to the same disk viewed through a spherical halo at inclination i'.

the ratios of the optical depths are proportional to the line segments N$'$P and F$'$P. From the elementary properties of the ellipse, it follows that the two ratios are the same (NP/FP = N$'$P/F$'$P). By straightforward trigonometry, one has $q\tan i = \tan i'$. In other words, the asymmetry signal of a flattened halo with axis ratio q is the same as that of an equivalent spherical halo, provided the disk is viewed not at angle i but at an angle i'.

This transformation takes into account the geometric effects of flattening. The first-order changes in the velocity distribution can be computed using the tensor virial theorem (Binney & Tremaine 1987; Han & Gould 1995). Strictly speaking, the tensor virial theorem applies globally and relates the components of the total kinetic energy tensor T to the components of the total potential energy tensor W. If we assume that the virial theorem holds at each spot, then it follows that

$$\frac{\sigma_x^2}{\sigma_z^2} \approx \frac{T_{xx}}{T_{zz}} = \frac{W_{xx}}{W_{zz}} \approx \frac{1}{q^2}\ . \tag{5}$$

Here, we have assumed that the figure is oblate spheroidal, with the short axis being in the z-direction and the (x, y)-plane being equatorial. Although this is only an approximate relation, valid for small flattening, it shows that the first-order changes in the velocity distribution are also accounted for by the transformation.

This means that a quick way to study the asymmetry properties of flattened halos is to take isotropic spherical models and vary the inclination angle of the M31 disk. We stress that the transformation does not allow us to calculate absolute quantities like the rate, but only the ratios of such quantities in the near and far disk.

3.2. *Results*

Figure 3 shows the variation in the far- to near-disk ratios for the pixel lensing rates A, the means of vertical distances D, and the timescales. The asymmetry signal A for a halo with flattening q is linearly related to the asymmetry signal

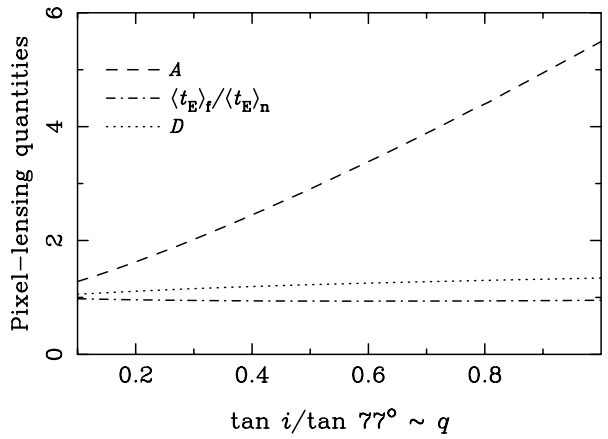


FIG. 3.—Far- to near-disk ratio for the pixel lensing rate A (*dashed line*), the mean vertical distance D (*dotted line*), and the timescales (*dot-dashed line*), shown as a function of flattening. This diagram is drawn using the transformation introduced in § 3.1.

for a spherical halo A_0; that is,

$$A \simeq 1 + q(A_0 - 1) \, . \tag{6}$$

The asymmetry signal clearly diminishes with flattening; it is obvious that, in the completely flat limit where the halo becomes a razor-thin disk, the asymmetry must vanish. The change in A with flattening is almost entirely caused by the change in the ratio of optical depths. Therefore, the ratio of the average timescales is largely unaffected by flattening.

The distance asymmetry D also decreases with increasing flattening, as is again obvious in the razor-thin limit. The distance asymmetry arises in a spherical model as a result of two effects. First, lines of sight are longer as we move from the near to the far disk. Second, the line of sight with the greatest column density goes through the center in the near disk but lies away from the center in the far disk. Thus, the distribution of distances of events is monotonically decreasing in the near disk but rises to a maximum and then decreases in the far disk. As the flattening increases, all lines of sights become shorter, and the density becomes more concentrated toward the center. The distributions of distances in both the near and far disk shrink, and the maximum moves toward the center in the far disk. This latter effect is the dominant one, and so the distance asymmetry signal falls with increasing flattening.

4. SIGNAL DETECTION

4.1. *The Number Asymmetry Signal*

In this section, we ask whether one can detect the asymmetry signals in the presence of contaminating events and how the velocity anisotropy and the halo flattening affect this detectability. That is, we ask how many candidates are needed to detect the asymmetry at a certain confidence level.

First, we consider the number asymmetry A between the far and near side. One problem is that none of the experiments will be able to obtain pure samples of M31 MACHO events; some microlensing contamination from Milky Way MACHOs and M31 stars, as well as nonmicrolensing contamination from variable stars and supernovae in background galaxies, will be inevitable. Contamination by periodic variables can be minimized by observing over a sufficiently long time. Color information can also be used to eliminate variable stars. Fortunately, the other contaminants are equally likely to occur in the near and far regions of the M31 disk. Whether an asymmetry can be detected is therefore a question of the size of the sample, the magnitude of the underlying M31 MACHO asymmetry, and the level of contamination.

Let us denote the numbers of M31 MACHO events in the near and far disk by N_n and N_f, respectively, and the number of contaminants by N_c. The condition for a detection of the asymmetry signal at the $s\ \sigma$ level is that the difference between the far and the near counts be greater than s times the Poisson error, which is given by the square root of the total number of the events. Therefore,

$$\frac{N_f' - N_n'}{\sqrt{N_f + N_n + N_c}} > s \, , \tag{7}$$

where N_f' and N_n' are the total number of candidates on the far and near sides, respectively, including contaminant events. In the case in which the contaminants are distributed evenly between the far and near disk, $N_f' - N_n' = N_f - N_n$. Straightforward manipulation of the above condition leads to a condition on the total number of candidate events,

$$N_t > s^2 \left(\frac{A+1}{A-1} \right)^2 (1 + f_c)^2 \, , \tag{8}$$

where $A = N_f/N_n$ is the underlying asymmetry of the M31 MACHO events, $f_c = N_c/(N_f + N_n)$ is the contamination factor, and $N_t = N_f + N_n + N_c$ is the total number of candidate events. Figure 4 shows the expected number of events (including the contaminants) required to detect an asymmetry at the 99% confidence level ($s = 2.58$) for various contamination factors. We see immediately that the size of the asymmetry signal is crucial. If $A \lesssim 2$, then even with low contamination the number of M31 microlensing events needed to give a convincing detection of asymmetry exceeds 60. On the other hand, if the asymmetry is ~ 5, then more than 15 candidates are required. Reassuringly, on referring to Figures 1 and 3, we see that A typically lies between 5 and 7

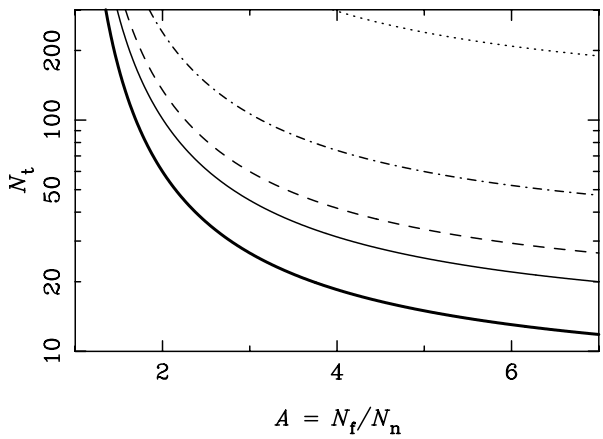


FIG. 4.—Number of candidate events (M31 MACHOs and contaminants) required to confirm asymmetry with 99% confidence, based on number count information alone, plotted as a function of the underlying M31 MACHO number asymmetry A. The different lines correspond to contamination factors: $f_c = 0$ (*thick solid line*), 0.3 (*thin solid line*), 0.5 (*dashed line*), 1 (*dot-dashed line*), and 3 (*dotted line*).

for spherical models and only becomes as small as 2 for models with $q = 0.3$. In fact, halos flatter than this are not likely on dynamical grounds, as they are susceptible to bending instabilities (e.g., Merritt & Sellwood 1994). Samples of $\sim$15 candidate events are well within the reach of the current surveys if MACHOs contribute significantly to the dark matter budget. However, this number is only the contribution of the M31 halo, as we have cut out the central parts of the M31 disk.

If the contribution of MACHOs to the dark matter mass budget is significant in M31, we expect a similar MACHO contribution for the Milky Way. For interesting MACHO fractions, the foreground Milky Way MACHOs may well provide the dominant contribution to f_c. If the typical MACHO mass and halo density contributions are universal, then the magnitude of f_c will be determined, to first order, by the relative masses of the M31 and Milky Way halos. If the M31 halo is twice as massive as that of the Milky Way, then $f_c \sim 0.4$ (Kerins et al. 2001), while we should expect f_c to be closer to unity if the two halos are equally massive (Evans & Wilkinson 2000). In any case, the total number of candidates required to confirm asymmetry scales as $(1 + f_c)^2$ from equation (8), so we require 4 times as many candidates to detect the asymmetry when $f_c = 1$ as when $f_c = 0$.

4.2. *The Distance Asymmetry Signal*

Motivated by the variation in mean distances of events between the near and far disk seen in Figures 1 and 3, we can go beyond the asymmetry in number counts by considering a distance asymmetry signature.

To quantify differences between the near-disk and far-disk event positions, we apply the Mann-Whitney rank sum test (Mann & Whitney 1947). This is a nonparametric test for differences between the medians of two samples. The Mann-Whitney test exploits the fact that two samples drawn from identical distributions exhibit the property that, if one combines them and then ranks the elements by size, the two samples are uniformly intermingled on average within the ranked combined sample. For two samples of large enough size n_a and n_b, the sum of the rank numbers for sample a is normally distributed about a mean $\mu_a = n_a(n_a + n_b)/2$ with a variance $\sigma_a^2 = n_a n_b(n_a + n_b + 1)/12$. The null hypothesis of similarity (or, in our case, symmetry) is therefore straightforward to quantify.

In the case of M31 pixel lensing, we can apply the Mann-Whitney test to the distribution of y, the projected distance from the M31 major axis, for candidates in the near- and far-disk subsamples. We can also combine the Mann-Whitney test with the number asymmetry test, since the Mann-Whitney statistic probes the spatial distribution of events, not the relative sizes of the samples. If the far-disk event positions are designated as sample a and the sum of their rank numbers within the combined near- and far-disk sample is θ_a, then we can define $s_{\rm MW} = (\theta_a - \mu_a)/\sigma_a$. Taking s_N to be the significance of the number asymmetry statistic, as defined by the left-hand side of equation (7), the overall significance of the combined sample is $s = (s_{\rm MW}^2 + s_N^2)^{1/2}$. A value of $s = 2.58$ would indicate a near-far asymmetry favored at the 99% confidence level.

We have performed Monte Carlo simulations to determine the number of candidates required to secure a 99% confidence detection of asymmetry. The simulations test a range of anisotropic and flattened halo models and a range of contaminations. For a given model, event position realizations are generated using the theoretical pixel lensing rate of equation (3), weighted by source number density. For each new event realization, the overall significance s of the cumulative sample is computed from both the Mann-Whitney statistic ($s_{\rm MW}$) and the number asymmetry statistic (s_N). When there are fewer than five events in either the far- or near-disk subsamples, only the number asymmetry statistic is used because the distribution of rank sums for small data sets can deviate strongly from Gaussianity. We assume the contaminating populations are symmetrically distributed about the M31 major axis, although we adopt the most difficult case when they have a comparable spatial dispersion to the M31 MACHO events. The extent to which this is true depends on whether Milky Way MACHOs, on the one hand, or variable stars and stellar microlenses, on the other hand, provide the dominant contribution to N_c. If the latter population dominates, then contaminants are likely to be more spatially concentrated than M31 MACHOs, making the MACHO asymmetry easier to measure for a given f_c. So for each pixel lensing realization, a uniform random number in the interval [0, 1] is chosen. If it is less than $f_c/[2(1 + f_c)]$, then the position of the event is flipped about the M31 major axis. This means that, on average, a fraction $f_c/(1 + f_c)$ of the total sample is symmetrically distributed, as required. A full trial, i, is terminated either when the cumulative sample of $N_{t,i}$ candidates provides at least a 99% confidence detection of asymmetry, or when the program estimates that the required sample is likely to exceed 500 events. This whole process is repeated 1000 times for each model, and the median value of $N_{t,i}$ (excluding trials that are prematurely terminated) is adopted as the estimate for N_t.

The top panel of Figure 5 shows the median number of candidate events (including the contaminants) required to detect an asymmetry with 99% confidence, as a function of the halo velocity anisotropy parameter α. In the absence of contamination, a sample size between 11 and 14 events is typically sufficient to detect asymmetry. The raggedness of this line is partly due to Monte Carlo noise but also partly due to the fact that N_t necessarily takes only a few discrete values in the limit of small data sets. From equation (7), the smallest sample needed give rise to a 99% confidence detection of asymmetry is seven events, all of which must be located in the far disk (assuming the asymmetry is caused by M31 MACHOs). When one candidate lies in the near disk we need $N_t = 11$, and when two candidates lie in the near disk we require $N_t = 14$. The leaps in the thick solid line between 11 and 14 events reflect this discrete behavior, although the oscillation back and forth for $-2 < \ln(1 + \alpha) < -1$ is due to Monte Carlo noise. In the worst case, considered in Figure 5, in which contaminants outnumber M31 MACHOs by 3 : 1, a median sample of $\sim$120 events is required to detect asymmetry. For $\alpha = 0$ and $f_c = 3$, we find that the expectation value of N_t is around 190. Using $s = 2.58$, $f_c = 3$, and an asymmetry $A = 5.5$ when $\alpha = 0$ (Fig. 1), equation (8) indicates that we should require $N_t = 220$ if we use number count information alone. Therefore, the addition of distance information allows around a 15% reduction in the required number of candidates in this case.

Overall, N_t does not appear to be particularly sensitive to α. This is to be expected when contamination levels are high, because the 30% contrast in A between the radially

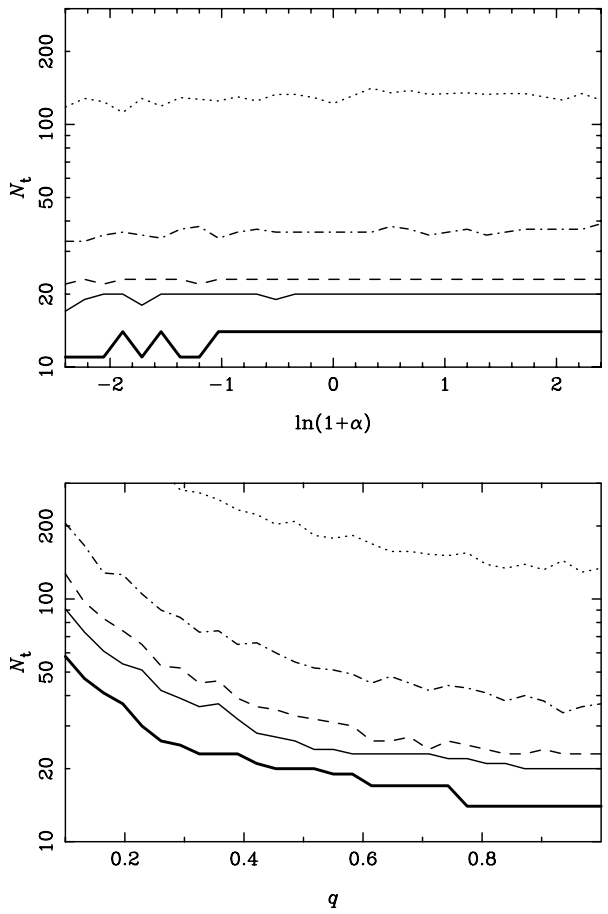


FIG. 5.—Median number of candidates (M31 MACHOs and contaminants) required for a 99% confidence detection of asymmetry. Line coding is the same as in Fig. 4. *Top*: Shows N_t as a function of halo velocity anisotropy for a spherical halo. *Bottom*: Shows N_t for flattened halo models, using the equivalence between the halo flattening parameter q and disk inclination i discussed in § 3.1.

and circularly anisotropic models (see Fig. 1) is strongly diluted.

The bottom panel of Figure 5 shows the situation for flattened halo models. The larger range in A for the flattened models ($1.3 < A < 5.5$) means that the median N_t shows a greater sensitivity to flattening than to velocity anisotropy. In the absence of contaminants, $N_t \lesssim 25$ is typically needed to confirm asymmetry for models rounder than $q = 0.3$. A sample of 100 candidates would permit asymmetry to be detected even if $f_c \simeq 1$. Adding distance information is particularly effective at reducing the required size of candidate samples for highly flattened models. As an extreme example, when $q = 0.1$ and $f_c = 0$, the expectation of N_t is around 80 if distance information is used along with number counts. From equation (8), 750 candidates are required if only number counts are used. This shows the value of the Mann-Whitney statistic.

It is, of course, much more difficult to measure an asymmetry than to detect one. Suppose an experiment has gathered $N_t \gtrsim 100$ events (including contaminants). With reference to Figure 4, if there has been no detection of asymmetry at the 99% confidence level, then—as $A \gtrsim 3$ for all models we have considered with $q > 0.5$—we can infer that the signal has been overwhelmed by contaminants ($f_c > 1$). The degree of contamination must be greater than a critical value, which is given by computing the curve that passes through the point $(A = 3, N_t)$. So, a null signal can be used to give a constraint on the contamination. On the other hand, if there has been a detection, then the measured signal $A' \simeq (N_f + \frac{1}{2}N_c)/(N_n + \frac{1}{2}N_c)$ is merely a lower limit to the true signal. It should be possible to estimate the contamination fraction statistically even if we do not know the individual contaminating events, so the true asymmetry signal can be matched to models using standard Bayesian likelihood methods (Kerins et al. 2001). Current surveys should therefore be able to discriminate between halo models with different degrees of flattening and may, if the spatial distribution of contaminant populations is well characterized, be able to distinguish between radially anisotropic halo models and tangentially anisotropic or isotropic models.

4.3. *Confusion from M32 and its Stream*

Additional confusion of the asymmetry signal may come from microlensing by stars that belong to streams or tidal debris from disrupted satellite galaxies cannibalized by M31 and/or by stars belonging to the intervening dwarf elliptical M32.

Ibata et al. (2001) have traced out a giant stream in the M31 stellar halo in red giant branch star counts. The stream is $\sim 1^\circ$ wide in projection. It seemingly originates from the satellite galaxy M32 and possibly also incorporates NGC 205. The average surface brightness of the stream is ~ 30 mag arcsec^{-2} in the V band. It has been suggested by Ferguson et al. (2002) that this may confuse the detection of the near-far disk asymmetry in the microlensing experiments. For sources in M31 and lensing populations at roughly the same distance from the sources, the optical depth of the stream is

$$\tau \sim 4.3 \times 10^{-10} \left(\frac{d}{20\ \mathrm{kpc}}\right) \left(\frac{M/L}{M_\odot/L_\odot}\right) 10^{(12-0.4\,\mu)}\,, \quad (9)$$

where μ is the surface brightness in magnitudes per square arcsecond, d is the separation of the stream from the M31 disk along the line of sight, and M/L is the MACHO mass-to-light ratio of the stream. This ratio must exceed 100 for the optical depth of the stream to be comparable to the other lensing populations. Accordingly, the presence of such streams is not likely to be problematic for asymmetry detection.

More problematic may be the intervening dwarf elliptical galaxy M32. The POINT-AGAPE collaboration has already found a candidate that lies $\sim 3'$ in projection away from the center of M32 and argued that the lens most probably lies in M32 itself (Paulin-Henrikkson et al. 2002). The optical depth of M32 is estimated to be (Paulin-Henrikkson et al. 2003)

$$\tau \sim 1.4 \times 10^{-6} \left(\frac{d}{20\ \mathrm{kpc}}\right) \left(\frac{M/L}{3\ M_\odot/L_\odot}\right)\,, \quad (10)$$

where d is the separation of M32 from M31 along the line of sight and M/L is the stellar mass-to-light ratio of M32. This is comparable to the signal expected from the baryonic halo (assuming a 20% MACHO fraction). Although microlensing associated with M32 is a potentially significant contaminant, the affected region can be readily excluded from the statistics using an appropriate mask.

5. CONCLUSIONS

Pixel lensing experiments targeting M31 are hoping to exploit the favorably high disk inclination in order to detect an asymmetry in the spatial distribution of microlensing events. If such a signal is found, it will provide powerful evidence for the existence of MACHOs.

For a spherically symmetric and isotropic halo, the numbers of M31 MACHOs in the far disk outnumber those in the near disk by more than 5 to 1. This asymmetry is increased by about 30% if M31 MACHOs occupy radial orbits rather than tangential ones. The signal is diminished if M31 MACHOs lie in a flattened halo. However, even for halos as flat as $q = 0.3$, the numbers of M31 MACHOs in the far side will outnumber those in the near side by a factor of $\sim$2.

The key to detecting asymmetry is to isolate microlensing events solely due to M31 MACHOs. There is likely to be significant contamination from other microlensing populations, as well as from variable stars and supernovae mistaken for microlensing, which will dilute the observed signal. The combination of number count and distance information permits asymmetry to be detected for a wide range of halo models, even in the presence of significant levels of contamination. For models with high levels of asymmetry, such as spherical halos or halos with a high degree of radial velocity anisotropy, number count information alone provides a sensitive diagnostic. The addition of distance information allows an $\sim$15% reduction in the size of samples needed to confirm asymmetry. For models with low levels of asymmetry, such as strongly flattened halos, distance information can reduce the required size of candidate samples by a factor of 2 or more.

A sample of 50 events is typically sufficient to detect asymmetry in the M31 MACHO distribution within spherical halos, even if only half the sample is due to M31 MACHO events. For flattened halo models, a sample of 50 candidates would likely allow asymmetry to be seen, provided the halo axis ratio $q \geq 0.3$ and the contaminants do not contribute more than a third of the sample. The term "contaminants" covers Milky Way MACHOs, M31 disk stellar lensing events, and variable star populations, all of which are assumed to be symmetrically distributed with respect to the major axis. For comparison, Paulin-Henriksson et al. (2003) have already found 362 light curves compatible with microlensing from the first 2 years of the POINT-AGAPE survey, although the contamination factor may still be very large. Samples of 50 events with modest contamination are easily achievable with the current generation of pixel lensing surveys.

N. W. E. and J. A. thank the Royal Society and the Leverhulme Foundation, respectively, for financial support.

REFERENCES

Ansari, R., et al. 1997, A&A, 324, 843
Aurière, M., et al. 2001, ApJ, 553, L137
Bahcall, J. N., & Soneira, R. M. 1980, ApJ, 238, L17
Baillon, P., Bouquet, A., Giraud-Héraud, Y., & Kaplan, J. 1993, A&A, 277, 1
Baltz, E., Gyuk, G., & Crotts, A. 2003, ApJ, 582, 30
Binney, J., & Tremaine, S. 1987, Galactic Dynamics (Princeton: Princeton Univ. Press)
Calchi-Novati, S., et al. 2002, A&A, 381, 848
Crotts, A. P. S. 1992, ApJ, 399, L43
———. 2001, in ASP Conf. Ser. 239, Microlensing 2000: A New Era of Microlensing Astrophysics, ed. J. W. Menzies & P. D. Sackett (San Francisco: ASP), 318
Crotts, A. P. S., & Tomaney, A. B. 1996, ApJ, 473, L87
Emerson, D. T. 1976, MNRAS, 176, 321
Evans, N. W., Häfner, R. M., & de Zeeuw, P. T. 1997, MNRAS, 286, 315
Evans, N. W., & Wilkinson, M. 2000, MNRAS, 316, 929
Ferguson, A. M. N., Irwin, M. J., Ibata, R. A., Lewis, G. F., & Tanvir, N. R. 2002, AJ, 124, 1452
Han, C., & Gould, A. 1995, ApJ, 449, 521
Ibata, R. A., Irwin, M. J., Lewis, G. F., Ferguson, A. M. N., & Tanvir, N. R. 2001, Nature, 412, 49
Kerins, E. J. 2001, in Cosmological Physics with Gravitational Lensing, ed. J. Trân Thanh Vân, Y. Mellier, & M. Moniez (Les Ulis: EDP Sciences), 43
Kerins, E. J., et al. 2001, MNRAS, 323, 13
Kiraga, M., & Paczyński, B. 1994, ApJ, 430, L101
Mann, H., & Whitney, D. 1947, Ann. Math. Statist., 18, 50
Merritt, D., & Sellwood, J. A. 1994, ApJ, 425, 551
Paczyński, B. 1986, ApJ, 304, 1
Paulin-Henriksson, S., et al. 2002, ApJ, 576, L121
———. 2003, A&A, 405, 15
Riffeser, A., et al. 2001, A&A, 379, 362
Walterbos, R., & Kennicutt, R. 1987, A&AS, 69, 311
White, S. D. M. 1981, MNRAS, 195, 1037
Wielen, R., Jahreiss, H., & Krüger, R. 1983, in Proc. IAU Colloq. 76, The Nearby Stars and the Stellar Luminosity Function, ed. A. G. Davis Philip & A. R. Upgren (Schenectady: L. Davis Press), 163